Involvement of the TCR Cβ FG Loop in Thymic Selection and T Cell Function

Tetsuro Sasada,[1,2] Maki Touma,[1,2] Hsiu-Ching Chang,[1,2] Linda K. Clayton,[1,2] Jia-huai Wang[1,3,4] and Ellis L. Reinherz[1,2]

[1]*Laboratory of Immunobiology, Dana-Farber Cancer Institute, and* [2]*Department of Medicine,* [3]*Department of Pediatrics, and* [4]*Department of Biological Chemistry and Molecular Pharmacology, Harvard Medical School, Boston, MA 02115*

Abstract

The asymmetric disposition of T cell receptor (TCR) Cβ and Cα ectodomains creates a cavity with a side-wall formed by the rigid Cβ FG loop. To investigate the significance of this conserved structure, we generated loop deletion (βΔFG) and βwt transgenic (tg) mice using the TCR β subunit of the N15 CTL. N15βwt and N15βΔFG H-2^b animals have comparable numbers of thymocytes in S phase and manifest developmental progression through the $CD4^-CD8^-$ double-negative (DN) compartment. N15βΔFG facilitates transition from DN to $CD4^+8^+$ double-positive (DP) thymocytes in recombinase activating gene (RAG)-$2^{-/-}$ mice, showing that pre-TCR function remains. N15βΔFG animals possess ~twofold more $CD8^+$ single-positive (SP) thymocytes and lymph node T cells, consistent with enhanced positive selection. As an altered Vα repertoire observed in N15βΔFG mice may confound the deletion's effect, we crossed N15αβ TCR tg RAG-$2^{-/-}$ with N15βΔFG tg RAG-$2^{-/-}$ H-2^b mice to generate N15αβ RAG-$2^{-/-}$ and N15αβ.βΔFG RAG-$2^{-/-}$ littermates. N15αβ.βΔFG RAG-$2^{-/-}$ mice show an 8–10-fold increase in DP thymocytes due to reduced negative selection, as evidenced by diminished constitutive and cognate peptide-induced apoptosis. Compared with N15αβ, N15αβ.βΔFG T cells respond poorly to cognate antigens and weak agonists. Thus, the Cβ FG loop facilitates negative selection of thymocytes and activation of T cells.

Key words: negative selection • thymocyte development • TCR structure • Ig superfamily • transgenic mice

Introduction

The TCR is a multicomponent complex composed of a Ti disulfide-linked heterodimer in noncovalent association with the CD3 subunits (1–5). The majority of T cells express a Ti-encoded by α and β TCR genes (Tiαβ) whereas a numerically minor but functionally significant subset expressed Ti encoded by γ and δ TCR genes (Tiγδ; for a review, see reference 6). The Tiαβ heterodimer whose overall shape and architecture are similar to an antibody Fab fragment represents the peptide–MHC complex (pMHC)* ligand binding unit. Thus, Ti αβ determines the ligand specificity of an individual T cell. In contrast, the CD3 polypeptides mediate TCR-based signal transduction. The signaling function of the CD3 components involves a conserved motif, termed immunoreceptor tyrosine-based activation motif (ITAM), present at 1–3 copies in the cytoplasmic domain of each CD3 subunit (7–9). The various CD3 subunits exhibit different interactions with intracellular signaling factors and, acting in concert, lead to T cell activation (10–15). However, how pMHC ligand binding to a Tiαβ or Tiγδ heterodimer subsequently initiates signaling via the CD3 molecules is currently unknown.

The TCR complex contains one copy of CD3γ and CD3δ and two copies of CD3ε and CD3ζ configured as two CD3εγ and CD3εδ heterodimers and a disulfide-linked CD3ζ homodimer (16–21). Recent crystallographic analysis (22) in conjunction with epitope mapping of a class I–restricted TCR (23) have identified a cavity within the Ti αβ constant (C) module of sufficient size to accommodate one nonglycosylated CD3ε ectodomain. In this regard, the solution structure of a heterodimeric CD3εγ

Address correspondence to Dr. Ellis L. Reinherz, Dana-Farber Cancer Institute, 44 Binney St., Boston, MA 02115. Phone: 617-632-3412; Fax: 617-632-3351; E-mail: ellis_reinherz@dfci.harvard.edu

**Abbreviations used in this paper:* aa, amino acid; APL, altered peptide ligand; BrdU, bromodeoxyuridine; DN, double negative; DP, double positive; PI, propidium iodide; pMHC, peptide–MHC complex; RAG, recombinase activating gene; SP, single positive.

 J. Exp. Med. © The Rockefeller University Press • 0022-1007/2002/06/1419/13 $5.00
Volume 195, Number 11, June 3, 2002 1419–1431
http://www.jem.org/cgi/doi/10.1084/jem.20020119

ectodomain complex reveals a unique side-to-side hydrophobic interface between the two C2-set immunoglobulin-like domains and indicates that a modular pair-wise association is shared between CD3εδ as well (24). CD3ε has an elongated shape with length, width and depth being ~40, 25, and 25 Å, respectively.

Herein, we have investigated the biological significance of the unusual structural arrangement of the Cβ FG loop that forms the side wall of this C-module cavity. Mapping studies using the Cβ FG loop-specific mAb H57 previously showed that one of two CD3ε subunits resides adjacent to this structural element. To this end, we have created TCR transgenic mice bearing either intact or Cβ FG loop-deleted β chains. Our results show that the loss of the Cβ FG loop attenuates negative selection without blocking positive selection within the thymus at the level of double-positive (DP) thymocytes. The sensitivity of mature T cells to cognate peptides as well as altered peptide ligands is also reduced. In contrast, pre-TCR facilitated transition from $CD44^{-}CD25^{+}$ to $CD44^{-}CD25^{-}$ double-negative (DN) thymocytes and subsequent DP thymocyte generation is not altered. The implications of these findings for TCR and pre-TCR function are discussed.

Materials and Methods

T Cell Receptor Construct. The FG loop-deleted mutant of the N15 TCRβ chain constant region (Cβ) was generated by PCR using N15β wt cDNA as a template, subcloned into the pCRII vector, and verified by DNA sequencing analysis. The StuI digested DNA fragment containing the FG loop-deleted constant region of the TCRβ chain was subcloned into the StuI site in the constant region of an N15 TCRβ expression vector, which was previously used for the generation of N15 TCRαβ tg recombinase activating gene (RAG)-$2^{-/-}$ H-2^{b} mice (25).

Mice. Mice transgenic for the N15 wt or FG loop-deleted TCRβ chain (hereafter for simplicity referred to as N15βwt or N15βΔFG) were produced in the transgenic/gene targeting core facility at Dana-Farber Cancer Institute. The N15 TCRβ shuttle constructs with the wt or FG loop-deleted mutant Cβ were digested with PvuI/SalI, leaving the bacterial vector sequences attached to the TCR gene. These DNAs were injected into (SJL × C57BL/6) F1 fertilized eggs and implanted into foster mothers. Resulting progeny were screened for integration of the N15 wt or FG loop-deleted TCRβ chain DNA by Southern blot analysis of tail DNA and by FACS® analysis of N15 TCRβ chain expression in peripheral blood nucleated cells. Five transgenic founders were identified, two for N15βwt, and three for N15βΔFG. The mice were backcrossed for 4–5 generations onto the C57BL/6 background before the experiments described below. To create N15βΔFG RAG-$2^{-/-}$ mice, the N15βΔFG mice were bred with RAG-$2^{-/-}$ C57BL/6 mice and the heterozygous N15βΔ$FG^{+/-}$ RAG-$2^{+/-}$ F1 mice were intercrossed and offspring which were N15βΔFG^{+}RAG-$2^{-/-}$ subsequently selected. The expression of the FG loop-deleted N15β chain and lack of RAG-2 were confirmed based on the Southern blot analysis of tail DNA and FACS® analysis of peripheral blood cells. To introduce the N15α chain into N15βΔFG mice and generate Ag-specific T cells with the FG loop-deleted TCRβ chain, the N15βΔFG RAG-$2^{-/-}$ (N15βΔ$FG^{+/-}$RAG-$2^{-/-}$) mice were bred with N15 TCRαβ tg RAG-$2^{-/-}$ H-2^{b} (N15α $wt^{+/+}$βwt$^{+/+}$ RAG-$2^{-/-}$ H-2^{b}) mice, and the resulting N15αwt$^{+/-}$βwt$^{+/-}$RAG-$2^{-/-}$ H-2^{b} or N15αwt$^{+/-}$ βwt$^{+/-}$βΔ$FG^{+/-}$RAG-$2^{-/-}$ H-2^{b} (hereafter for simplicity referred to as N15αβ or N15αβ.βFG mice) were used for the experiments. RAG-$2^{-/-}$ C57BL/6 mice were purchased from Taconic. All lines were maintained and bred under sterile barrier conditions at the animal facility of Dana-Farber Cancer Institute.

Peptide Synthesis. Peptides were synthesized by standard solid phase methods on an Applied Biosystems 430A synthesizer at the Biopolymers Laboratory of the Massachusetts Institute of Technology. All peptides were purified by reverse phase HPLC (Hewlett Packard HPLC 1100) with a C4, 2-mm column. Peptides were analyzed for purity and correct molecular weight by electrospray mass spectrometry, amino acid (aa) analysis, and HPLC. Peptides are named to indicate the substituted aa and the position in the sequence of VSV8 (e.g., L4 denotes replacement of valine by leucine at the fourth residue of the VSV8 peptide). VSV8 is a cognate antigenic peptide agonist of the N15 TCR, which triggers thymic negative selection in N15 TCRαβ tg RAG-$2^{-/-}$ H-2^{b} mice, whereas L4 and K1 peptides are altered peptide ligands (APLs) of VSV8 and weak agonists of the N15 TCR, which induce positive selection in N15 TCRαβ tg RAG-$2^{-/-}\beta_2M^{-/-}$ H-2^{b} mice (26).

Antibodies and Flow Cytometric Analysis. The following mAbs were used: R-phycoerythrin (PE)- or Cychrome-conjugated anti–mouse CD4 (H129.19); FITC- or Cychrome-conjugated anti–mouse CD8α (53–6.7); Cychrome-conjugated anti-TCR Cβ (H57–597); PE-conjugated anti-CD25 (PC61); FITC-conjugated anti-CD44 (IM7); FITC-conjugated anti-Vβ5.1, 5.2 (MR9.4); biotin-conjugated anti-CD69 (H1.2F3); biotin-conjugated anti-Vα2 (B20.1), anti-Vα3.2 (RR3–16), anti-Vα8.3 (B21.14), anti-Vα11.1, 11.2 (RR8–1), PE-conjugated streptavidin (BD PharMingen). For flow cytometry, single cell thymocyte or lymph node suspensions were prepared in PBS containing 2% FCS and 0.05% NaN_3. Cells were stained at 5×10^{6} cells per ml in PBS-2% FCS and 0.05% NaN_3 containing the antibodies at saturating concentrations. Phenotypes and proportions of thymocyte and lymph node cell subsets were analyzed by two-color flow cytometry using a FACScan™ (Becton Dickinson) and the CELLQuest™ program. Dead cells were excluded from the analysis by forward and side scatter gating.

Bromodeoxyuridine Staining. Bromodeoxyuridine (BrdU) incorporation was examined according to the manufacturer's protocol (BrdU Flow Kit; BD PharMingen). Mice were administered two intraperitoneal injections of 1 mg of BrdU in PBS at 4 h intervals. After 18 h, thymocytes were fixed/permeabilized and stained with FITC-conjugated anti-BrdU mAb following treatment with 30 μg/ml DNase. Live cells were gated and analyzed on a FACScan™.

Apoptosis Assay. Thymocytes from untreated, VSV8 peptide-injected (0.5 μg intravenously, 18 h previously) or dexamethasone-treated (0.5 mg intraperitoneally, 6 h previously) were examined. Apoptosis of thymocytes was evaluated by cellular DNA content determined by propidium iodide (PI) staining and alterations in plasma membrane permeability examined by Annexin V staining. For PI staining, after fixation with 40% ethanol at 4°C for 30 min, total thymocytes (10^{6} cells) were resuspended in PBS containing 50 μg/ml RNase A and 2.5 μg/ml PI and incubated at 37°C for 30 min. PI incorporation was analyzed by flow cytometry. For annexin V staining, after washing with PBS, total thymocytes (10^{6} cells) were resuspended in 1× binding buffer containing 0.5 μg/ml FITC-conjugated annexin V (ApoAlert Annexin V Apoptosis kit; CLONTECH Laboratories,

Inc.) and 2.5 μg/ml PI to gate out dead cells, and incubated in the dark for 10 min at room temperature, followed by the analysis on a FACScan™.

Proliferation Assay. Lymph node cells from N15αβ or N15αβ.-βΔFG mice (10^5/well) were incubated at 37°C with 2×10^4 irradiated EL-4 thymoma cells, which had been preloaded for 2 h with the indicated doses of VSV8 or a weak agonist, L4, in AIM-V medium (Life Technologies) containing 50 μM 2-ME. After 48 h incubation, 0.4 μCi per well of [^{3}H]TdR (ICN Biomedicals) was added, and after an additional 18 h of culture at 37°C, the cells were harvested and the incorporated radioactivity was measured.

Measurement of IFN-γ. IFN-γ production was induced under the same culture conditions used for proliferation assays (see above). After 48 h of incubation, supernatants were collected and assayed for IFN-γ using a mouse IFN-γ ELISA kit (Mouse IFN-γ OptEIA Set; BD PharMingen). The sensitivity of the assay was 31.3–2,000 pg/ml and results were calculated as the mean of duplicate wells.

Results

The TCR Cβ FG Loop Structure and Sequence Comparison. One remarkable feature of the TCR Cβ domain is the striking elongation of the FG loop. Compared with other Ig-like structures (aside from the TCR Cγ domain), there is a 13 aa insertion within the FG loop (27). Fig. 1 A shows a view of the crystallographically resolved murine N15 class I MHC-restricted αβ TCR (Vβ5.2 D2Jβ2.6 Cβ2/Vα8 Jα5Cα; reference 22). The unique protrusion of the Cβ domain's FG loop is apparent (bracketed in a black box). It was previously noticed that internally the loop is well structured (22). The Trp225 at the tip of the loop

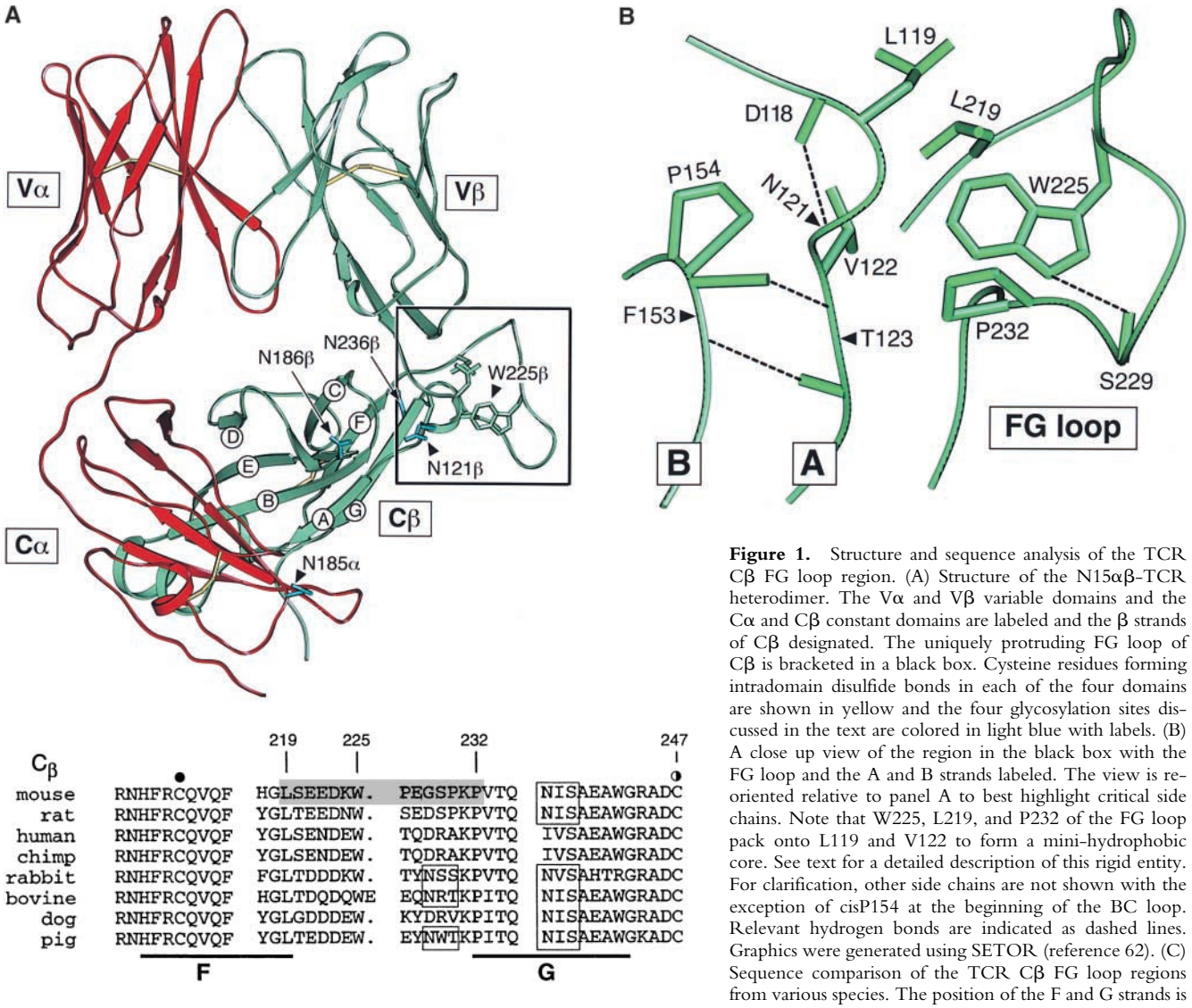

Figure 1. Structure and sequence analysis of the TCR Cβ FG loop region. (A) Structure of the N15αβ-TCR heterodimer. The Vα and Vβ variable domains and the Cα and Cβ constant domains are labeled and the β strands of Cβ designated. The uniquely protruding FG loop of Cβ is bracketed in a black box. Cysteine residues forming intradomain disulfide bonds in each of the four domains are shown in yellow and the four glycosylation sites discussed in the text are colored in light blue with labels. (B) A close up view of the region in the black box with the FG loop and the A and B strands labeled. The view is reoriented relative to panel A to best highlight critical side chains. Note that W225, L219, and P232 of the FG loop pack onto L119 and V122 to form a mini-hydrophobic core. See text for a detailed description of this rigid entity. For clarification, other side chains are not shown with the exception of cisP154 at the beginning of the BC loop. Relevant hydrogen bonds are indicated as dashed lines. Graphics were generated using SETOR (reference 62). (C) Sequence comparison of the TCR Cβ FG loop regions from various species. The position of the F and G strands is defined based on the above crystallographic analysis. The shaded region defines the 14 aa residue deleted from the N15 TCR β chain. Boxed residues mark the potential N-linked glycosylation signals. The β chain cysteine (247) which forms an interchain disulfide with the α chain, is indicated by the semi-solid circle and the F strand cysteine (212) which forms the intradomain disulfide with the β strand cysteine (147) of Cβ (not shown) is indicated by the solid circle.

plays a key role. A hydrogen bond between the NE1 of Trp225 and the carbonyl group of Ser229 brings the bulky indole ring of Trp225 in position to make hydrophobic contacts with Leu219 and Pro232 at the base of the FG loop (Fig. 1 B, a close up view of the local region shown in the black box of Fig. 1 A). The hydrophobic patch composed of these three FG loop residues packs onto Leu119 and Val122 at the beginning of the Cβ domain's A strand to form a mini-hydrophobic core. The Leu119 and Val122 themselves lie on a stable local strut created by a tight β turn between Asp118 and Asn121. Moreover, a pair of mainchain hydrogen bonds between Thr123 on the A strand and Phe153 at the end of the B strand further stabilizes the local structure. Collectively, the Cβ domain FG loop, albeit a long protrusion, is an integrated component of a rigid structural entity that connects the Vβ and Cβ domains. Not only are the residues mentioned above all invariant among mouse, rat, human, chimpanzee, rabbit, cow, dog, and pig as shown in the Fig. 1 C, but the three-dimensional structural feature depicted in Fig. 1 B is also conserved in all known TCR crystal structures, including class I MHC-restricted N15 and 2C from mouse (22, 28) and B7 from human (29), as well as the human class II MHC-restricted HA1.7 (30).

T Lineage Development in N15βΔFG Mice. To analyze the role of the Cβ FG loop in thymocyte development and mature T cell function in vivo, we established transgenic mice expressing the wild-type N15 TCRβ chain or an FG loop deletion variant lacking aa 219–232. For simplicity, these TCR transgenes will be referred to as N15βwt and N15βΔFG, respectively. The N15βwt subunit derives from the N15 $CD8^+$ cytotoxic T cell clone whose TCR is specific for the vesicular stomatitis virus nucleoprotein aa 52–59 (VSV8) (RGYVYQGL) bound to the MHC class I molecule $H\text{-}2K^b$ (31). T lineage cells from the thymus and lymph nodes of N15βΔFG mice were then directly compared with those of the N15βwt mice. Fig. 2 A shows a flow cytometric analysis of $CD8^+$ single-positive (SP) lymph node T cells from 1 of 2 representative N15βwt lines and 1 of 3 representative N15βΔFG lines. As expected, the anti-Cβ FG loop specific mAb H57 (22, 32) reacts with virtually all $CD8^+$ SP lymph node T cells in N15βwt tg mice but almost no $CD8^+$ SP lymph node T cells in N15βΔFG mice. Those few reactive T cells (6.8%) represent $CD8^+$ SP cells that have rearranged endogenous β chains due to incomplete TCRβ chain allelic exclusion by the N15β transgene, as previously reported in other transgenic systems (33). Fig. 2 A also indicates that despite the Cβ FG loop deletion, N15βΔFG tg animals, like N15βwt tg mice, predominantly express the transgenic Vβ5.2 gene as detected by the MR9.4 mAb.

Perhaps more importantly, as shown in Fig. 2 B and Table I, comparison of thymocyte subsets reveals substantial differences between the N15βwt and N15βΔFG tg mice. At 6–12 wk of age, for example, N15βΔFG mice show a subtle but significant reduction in the number of total thymocytes (N15βwt, $12.05 \pm 2.99 \times 10^7$ [$n = 10$]; N15βΔFG, $9.51 \pm 2.09 \times 10^7$ [$n = 15$], $P < 0.05$; Table I). Furthermore, as shown by the representative CD4/CD8α double-staining profiles in Fig. 2 B, there is a detectable increase in the percentage of the $CD8^+$ SP subset and a decrease in that of the DP subset in N15βΔFG thymocytes compared with N15βwt mice. Therefore, N15βΔFG mice show a statistically significant increase in the absolute number of $CD8^+$ SP thymocytes and a concommitant decrease in DP thymocytes (Table I). This increase in $CD8^+$ SP cells is further reflected by the increase in $CD8^+$ SP lymph node T cells (N15βwt, $1.99 \pm 0.77 \times 10^7$ [$n = 10$]; N15βΔFG $3.45 \pm 0.82 \times 10^7$ [$n = 15$]). From these findings, we conclude that the absence of the FG loop in the constant region of N15 TCR β chain influences T cell development in the tg mouse model.

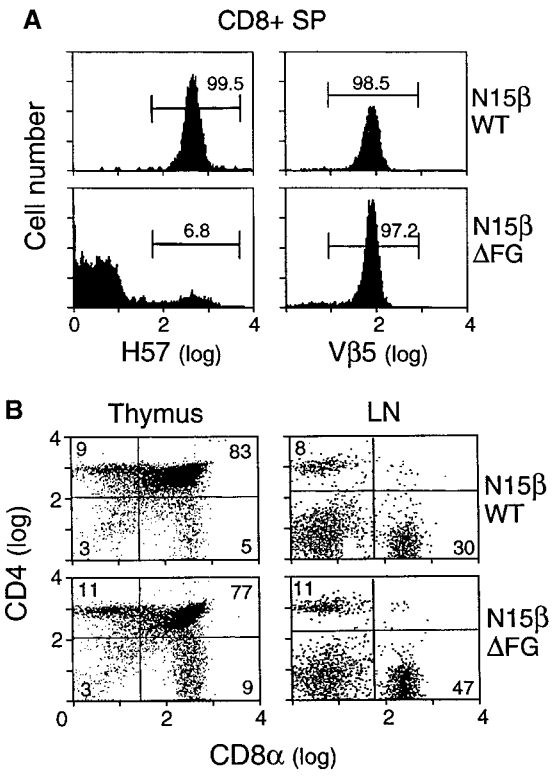

Figure 2. Altered phenotypes of T lineage cells in the N15βΔFG mice. (A) TCR expression on $CD8^+$ SP lymph node T cells in the N15βwt and N15βΔFG mice. Lymph node cells from 8-wk-old N15βwt and N15βΔFG mice were triple-stained with anti-CD4, anti-CD8, and anti-TCR Cβ FG loop specific H57 or anti-Vβ5 MR9.4 mAbs. The histograms of TCR Cβ FG loop (left) and Vβ5 (right) expression on the gated $CD8^+$ SP lymph node T cells are shown. The numbers represent the percentages of H57- or Vβ5-positive cells (as indicated). (B) The CD4/CD8α double-staining profiles in thymocytes and lymph node cells are altered by the lack of the TCR Cβ FG loop. The thymocytes and lymph node cells from N15βwt and N15βΔFG mice at 8 wk of age were double-stained with PE-anti-CD4 and FITC-anti-CD8α. The expression of CD4 (y axis) and CD8α (x axis) on thymocytes and lymph node cells was detected by flow cytometry after gating on 10,000 live cells. The percentages of each subset are indicated.

There are two major checkpoints at which αβ thymocyte development is dependent upon the TCR β chain. The earliest occurs during the transition from DN to DP thymocytes and is regulated by the pre-TCR complex

Table I. *Absolute Numbers of Total and Cell Subsets of Thymocytes and LN Cells in N15βwt and N15βΔFG Mice*

	Thymus					LN		
	Total[a]	DP[b]	CD8$^+$ SP[a]	CD4$^+$ SP	DN	Total	CD8$^+$ SP[c]	CD4$^+$ SP
N15βwt	12.05 ± 2.99[d]	9.95 ± 2.47	0.60 ± 0.17	1.08 ± 0.30	0.41 ± 0.16	6.36 ± 2.11	1.99 ± 0.77	0.49 ± 0.19
N15βΔFG	9.51 ± 2.09	7.31 ± 1.61	0.85 ± 0.29	1.02 ± 0.27	0.33 ± 0.12	7.17 ± 1.83	3.45 ± 0.82	0.71 ± 0.21

[a] $P < 0.05$.
[b] $P < 0.01$.
[c] $P < 0.0005$.
[d] The numbers of cell subsets in thymocytes and lymph node T cells were calculated by quantifying the total number of thymocytes and lymph node cells from 6–12-wk-old N15β ($n = 10$) and N15βΔFG ($n = 15$) mice and the percentages of each subset as determined by FACS® analysis. Results are expressed as mean ± SD ($\times 10^7$ cells). Statistical differences between N15βwt and N15βΔFG numbers in indicated populations are given.

comprised of the invariant pTα subunit disulfide linked to a TCR β chain in noncovalent association with the CD3 subunits (34). The later checkpoint involves the αβ TCR and occurs during the transition from DP to SP thymocyte maturation. At that time, self-MHC–restricted, nonautoreactive T cells are selected for maturation and peripheral exportation (35). To investigate the mechanism of the altered thymocyte phenotype in N15βΔFG mice, we first compared early thymic development in the N15βwt and N15βΔFG mice by examining the fraction of cells synthesizing DNA using BrdU incorporation in vivo. In this way, it is possible to test whether the FG loop deletion in the N15 TCRβ chain affects proliferation and/or turnover of thymocytes. The N15βwt and N15βΔFG tg mice were injected twice intraperitoneally with 1 mg of BrdU in PBS at 4 h intervals, and 18 h later, thymocytes were assayed for the incorporation of BrdU by flow cytometry. As shown in Fig. 3 A, the percentage of BrdU$^+$ thymocytes in the N15βΔFG mice was comparable to that observed in control N15βwt mice, indicating that the number of cells that had progressed through S phase is similar. In addition, we compared the developmental stages of immature thymocytes by examining the surface expression of CD25 and CD44 on DN thymocytes of these mice. The percentages of the four CD44/CD25 subsets (CD44$^+$CD25$^-$, CD44$^+$CD25$^+$, CD44$^-$CD25$^+$, and CD44$^-$CD25$^-$) in the N15βΔFG were equivalent to those of N15βwt mice (Fig. 3 B), suggesting that the deletion of Cβ FG loop from the N15 TCRβ chain does not disrupt the pre-TCR–facilitated transition from CD44$^-$CD25$^+$ to CD44$^-$CD25$^-$ DN thymocytes. To further assess the function of the Cβ FG loop-deletion in pre-TCR signaling at the CD44$^-$CD25$^+$ DN stage, we established RAG-2–deficient mice expressing the Cβ FG loop-deleted N15β chain (N15βΔFG RAG-2$^{-/-}$). Introduction of a functionally rearranged wild-type TCRβ chain overcomes the developmental arrest at the CD44$^-$CD25$^+$ DN stage observed in the RAG-2–deficient mice, leading to strong proliferation of DN thymocytes and efficient generation of DP cells (36). As shown in Fig. 3 C, N15βΔFG RAG-2$^{-/-}$ mice generate DP thymocytes with essentially normal cellularity

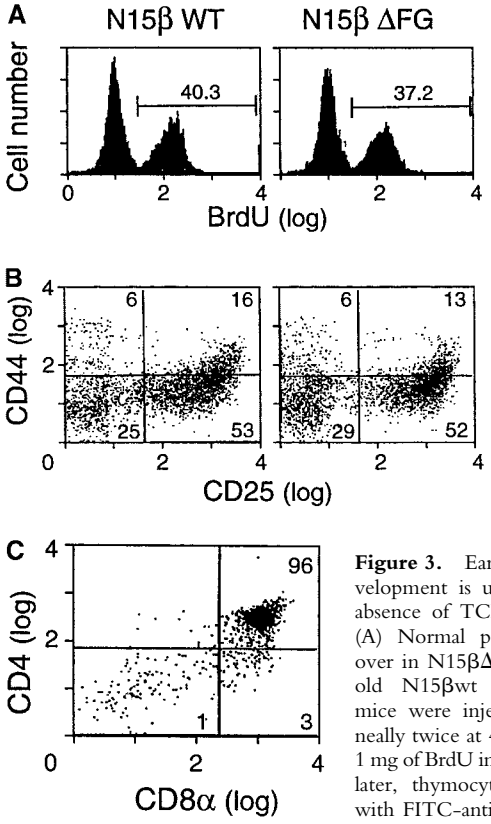

Figure 3. Early thymocyte development is unaffected by the absence of TCR Cβ FG loop. (A) Normal proliferation/turnover in N15βΔFG mice. 9-wk-old N15βwt and N15βΔFG mice were injected intraperitoneally twice at 4 h intervals with 1 mg of BrdU in 0.2 ml PBS. 18 h later, thymocytes were stained with FITC-anti-BrdU mAb and assayed by flow cytometry. The histograms of BrdU incorporation on 10,000 live thymocytes are shown. The numbers represent the percentages of BrdU-positive cells. (B) The transition from CD44$^-$CD25$^+$ to CD44$^-$CD25$^-$ DN thymocytes is not blocked in N15βΔFG mice. Total thymocytes were triple-stained with FITC-anti-CD44, PE-anti-CD25, and Cychrome-anti-CD4/anti-CD8α. The profiles of CD44 (y axis) versus CD25 (x axis) expression in Cychrome-negative (CD4$^-$CD8$^-$ DN) thymocytes are shown. The percentage of each subset is indicated. (C) Efficient generation of DP thymocytes in N15βΔFG RAG-2$^{-/-}$ mice. Thymocytes from 8-wk-old N15βΔFG RAG-2$^{-/-}$ mice were double-stained with PE-anti-CD4 and FITC-anti-CD8α. The expression of CD4 (y axis) and CD8α (x axis) on thymocytes was detected by flow cytometry after gating on 10,000 live cells. The percentages of each subset are indicated.

(6.6×10^7 thymocytes/mouse). These results suggest that signaling through the pre-TCR complex on $CD44^-$ $CD25^+$ thymocytes is not blocked by the deletion of the Cβ FG loop in the N15 TCRβ chain.

Altered Vα Usages by Peripheral Mature T Cells in the N15βΔFG Mice. Given the nearly twofold increase in the absolute number of $CD8^+$ SP lymph node T cells (Table I), we next examined whether deletion of the Cβ FG loop of the N15 β chain influences thymic repertoire selection. To this end, the TCR Vα gene usage of $CD8^+$ and $CD4^+$ SP lymph node T cells in N15βwt and N15βΔFG mice was assessed by flow cytometry using a panel of anti-Vα mAbs. As shown in Table II, there are statistically significant differences in the TCR Vα gene usage in peripheral lymph node T cells between N15βwt and N15βΔFG mice. $CD8^+$ lymph node T cells from N15βΔFG mice display an increased frequency of TCRs incorporating Vα8.3 (mean = 4.37%, SD = 0.58 versus mean = 3.74%, SD = 0.54; $P < 0.02$) and Vα11 (mean = 6.81%, SD = 0.70 versus mean = 5.46%, SD = 0.50; $P < 5 \times 10^{-5}$) gene segments compared with N15βwt mice (Table II). $CD4^+$ lymph node T cells from N15βΔFG mice also bear more TCRs incorporating Vα2 (mean = 13.61%, SD = 0.95 versus mean = 11.77%, SD = 1.38; $P < 0.005$) than those from N15βwt mice. These data suggest that lack of the Cβ FG loop exerts an influence on selection of the TCR repertoire by affecting usage of functional Vα gene segments, leading to the alterations in thymic and peripheral lymph node phenotypes observed in the N15βΔFG mice. That Vα differences are observed in $CD8^+$ SP thymocytes as well as lymph node cells is consistent with this view (data not shown), but does not exclude the possibility that impaired TCR signaling in the peripheral T cells in N15βΔFG animals further alters the repertoire.

Quantitative and Qualitative Alterations of Thymocytes and Peripheral T Cells in N15αβ.βΔFG Mice. The differences between N15βwt and N15βΔFG mice may have been modified by compensatory adaptations of Vα gene expression. To analyze more clearly the role of the TCR Cβ FG loop in thymocyte development and mature T cell function, we next crossed the N15βΔFG RAG-$2^{-/-}$ mice (N15βΔFG$^{+/-}$RAG-$2^{-/-}$ H-2^b) with N15αβ tg RAG-$2^{-/-}$ H-2^b (N15αwt$^{+/+}$βwt$^{+/+}$RAG-$2^{-/-}$ H-2^b) to generate two mouse strains: N15αwt$^{+/-}$βwt$^{+/-}$ RAG-$2^{-/-}$ and N15αwt$^{+/-}$βwt$^{+/-}$βΔFG$^{+/-}$RAG-$2^{-/-}$ mice. These mice are referred to hereafter for simplicity as N15αβ and N15αβ.βΔFG, respectively. In these strains, the TCRα chain is fixed and on the RAG-$2^{-/-}$ background, so no confounding endogenous β or α chains can be expressed.

T lineage cells from the thymus and lymph nodes of these animals are directly compared in Fig. 4, A and B. As defined by the anti-Vβ5 mAb MR9.4, using quantitative immunofluorescence on FACS®, the $CD8^+$ SP lymph node T cells from N15αβ.βΔFG mice expressed the same level of N15 β chain as $CD8^+$ SP T cells derived from N15αβ mice. However, the fluorescence intensity of anti-TCR Cβ H57 mAb staining in the $CD8^+$ SP T cells from N15αβ.βΔFG mice is ~50% that in N15αβ T cells, indicating that $CD8^+$ SP T cells from N15αβ.βΔFG mice express both wild-type and FG loop-deleted N15 TCRβ chains complexed with N15 TCRα chains at almost equal levels on their cell surface (Fig. 4 A). Although not shown, all peripheral T cells are $CD8^+$ SP in both N15αβ and N15αβ.βΔFG mice with equivalent surface CD8 density as revealed by the anti-CD8α mAb 53–6.7.

Comparison of the thymocyte cell number and subset distribution among N15αβ or N15αβ.βΔFG mice reveal striking differences. At 8–12 wk of age, N15αβ.βΔFG mice have a markedly larger thymus relative to that of N15αβ animals with an ~sevenfold increase in the number of total thymocytes (Fig. 4 C). Furthermore, as shown by the CD4/CD8α double-staining profiles in Fig. 4 B, there is a substantial increase in the DP subset percentage and a decrease in the DN and $CD8^+$ SP subset percentages in N15αβ.βΔFG thymocytes. As the total number of N15αβ.βΔFG thymocytes is ~7 times more than N15αβ thymocytes, N15αβ.βΔFG mice show no significant differences in the absolute numbers of DN and $CD8^+$ SP thymocytes, but ~10-fold more DP thymocytes than N15αβ mice (N15αβ, 1.48×10^7 DP cells versus N15αβ.βΔFG, 13.2×10^7 DP cells; Fig. 4 C). These results indicate that the absence of the TCR Cβ FG loop influences intrathy-

Table II. *Vα Usages by $CD8^+$ SP and $CD4^+$ SP Lymph Node Cells in N15βwt and N15βΔFG*

	$CD8^+$ SP				$CD4^+$ SP			
	Vα2	Vα3.2	Vα8.3[a]	Vα11[b]	Vα2[c]	Vα3.2	Vα8.3	Vα11
N15βwt	12.21 ± 0.95[d]	1.13 ± 0.43	3.74 ± 0.54	5.46 ± 0.50	11.77 ± 1.38	1.90 ± 0.46	2.00 ± 0.59	5.74 ± 1.54
N15βΔFG	12.19 ± 0.75	0.99 ± 0.38	4.37 ± 0.58	6.81 ± 0.70	13.61 ± 0.95	1.77 ± 0.58	2.35 ± 0.48	4.74 ± 1.04

[a] $P < 0.02$.
[b] $P < 0.00005$.
[c] $P < 0.005$.
[d] Lymph node cells from 6–12-wk-old N15β ($n = 10$) and N15βΔFG ($n = 15$) mice were stained with FITC anti-CD4, CyChrome anti-CD8, biotin anti-Vα mAb, followed by PE-conjugated streptavidin. Values represent the mean and SD of percentages in $CD8^+$ and $CD4^+$ SP lymph node T cell subsets as determined by FACS® analysis.

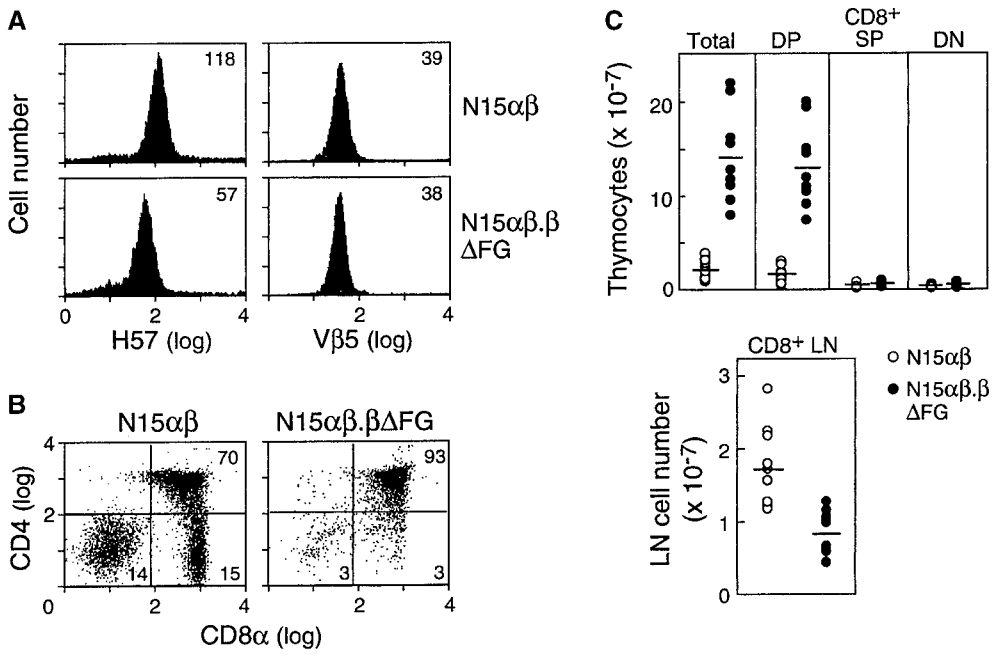

Figure 4. Quantitative and qualitative T lineage abnormalities in the N15αβ.βΔFG mice. (A) TCR expression on lymph node T cells in the N15αβ and N15αβ.βΔFG mice. Lymph node cells from 12-wk-old N15αβ and N15αβ.βΔFG mice were triple-stained with anti-CD4, anti-CD8, and anti-TCR Cβ FG loop-specific H57 or anti-Vβ5 MR9.4 mAbs. The histograms of TCR Cβ FG loop (left) and Vβ5 (right) expression on the gated $CD8^+$ SP lymph node T cells are shown. The numbers represent the values of mean fluorescence intensity. (B) The CD4/CD8α double-staining profile in thymocytes is altered in N15αβ.βΔFG mice. The thymocytes from N15αβ and N15αβ.βΔFG mice at 12 wk of age were double-stained with PE-anti-CD4 and FITC-anti-CD8α. The expression of CD4 (y axis) and CD8α (x axis) on thymocytes was detected by flow cytometry after gating on 10,000 live cells. The percentages of each subset are indicated. (C) The N15αβ.βΔFG mice show a drastic increase in the total and DP thymocytes, but a decrease in the $CD8^+$ SP lymph node T cells. The numbers of total, DP, $CD8^+$ SP, and DN thymocytes and $CD8^+$ SP lymph node T cells were calculated by quantifying the total numbers of thymocytes and lymph node cells from 8–12-wk-old N15αβ and N15αβ.βΔFG mice and the percentages of each subset as determined by FACS® analysis. Open circles (N15αβ mice [$n = 13$]) and closed circles (N15αβ.βΔFG mice [$n = 9$]) represent values of individual mice and bars represent average values for a given group. The total and DP thymocyte numbers are significantly higher, and $CD8^+$ SP lymph node cell number is significantly lower in the N15αβ.βΔFG mice, compared with the N15αβ mice (total and DP thymocytes, $P < 0.0001$; $CD8^+$ SP lymph node cells, $P < 0.0005$).

mic T cell development in the N15 TCR αβ tg mouse system. In contrast to the difference in thymocyte number, the number of peripheral $CD8^+$ SP lymph node T cells in N15αβ mice is ~2 times more than that in the N15αβ.βΔFG mice (N15αβ, 1.71×10^7 cells versus N15αβ.βΔFG, 0.87×10^7 cells). This difference in peripheral $CD8^+$ SP T cell number may result either from faulty homeostatic expansion of T cells in the peripheral lymphoid system of N15αβ.βΔFG mice as a consequence of impaired T cell activation (37) or represent a qualitative difference in $CD8^+$ SP thymocyte maturation and/or release into the peripheral T cell compartment. CFSE dye tracking of the $CD8^+$ SP transgenic T cells injected into B6 RAG-$2^{-/-}$ mice or irradiated B6 mice excludes detectable alteration in cell divisions, however (data not shown).

Decreased Thymic Negative Selection in the N15αβ.βΔFG Mice. The T cell repertoire is shaped by both negative and positive thymic selection processes acting primarily at the level of the immature DP thymocytes (for reviews, see references 35 and 38). Previous studies showed that DP thymocytes are deleted during negative selection via a caspase-dependent apoptotic mechanism (39). To investigate the basis for the dramatic increase in DP thymocytes in N15αβ.βΔFG, we evaluated the efficiency of the negative selection process in the N15αβ versus N15αβ.βΔFG animals. Apoptotic cells were enumerated through measurement of DNA content in total thymocytes using propidium iodide and flow cytometric analysis. As shown in Fig. 5 A, the percentage of thymocytes with subdiploid DNA content, a typical feature of apoptotic cell death, is significantly higher in the N15αβ mice than in the N15αβ.βΔFG mice (N15αβ, 12.5% versus N15αβ.βΔFG, 1.1%). Consistent with this result, alterations in plasma membrane permeability, one of the earliest changes in cells undergoing apoptosis, is also altered differentially in N15αβ versus N15αβ.βΔFG mice. As shown in Fig. 5 B, about half (48.5%) of the thymocytes in the N15αβ mice are positive for annexin V staining, suggesting that a large number of DP thymocytes are being continuously deleted by apoptosis. In contrast, only a small percentage (10.0%) of thymocytes are annexin V positive in N15αβ.βΔFG mice. This finding suggests that the nature of constitutive ongoing negative selection in DP thymocytes is different between N15αβ and N15αβ.βΔFG mice.

To further probe differences in the negative selection threshold of DP thymocytes from N15αβ and N15αβ.βΔFG mice, we injected the cognate peptide VSV8 intravenously and compared the phenotypic changes in thymocytes. 18 h after intravenous injection with 0.5 μg of VSV8 peptide, N15αβ mice showed an ~90% reduction in total thymocyte number (without VSV8 injection, 2.07×10^7 cells; after VSV8 injection, 0.26×10^7 cells), consistent with earlier observations (25). By contrast, there is no peptide-induced change in the total thymic cellularity in N15αβ.βΔFG mice (without VSV8 injection, 10.4×10^7 cells; after VSV8 injection, 10.6×10^7 cells). These re-

sults suggest that deletion of the Cβ FG loop alters the sensitivity of immature DP thymocytes to negative selection induced by the cognate peptide in N15 TCRtg mice. Consistent with the thymic cellularity data, DNA staining with propidium iodide shows a significant increase in the percentage of subdiploid DNA-containing cells after VSV8 injection in the N15αβ (35.8%) but not in the N15αβ.βΔFG mice (1.3%; Fig. 5 A). Furthermore, as shown in Fig. 5 B, the N15αβ mice display a prominent increase in the annexin V^+ thymocytes after 18 h of VSV8 (80.4%), compared with N15αβ.βΔFG mice (14.7%).

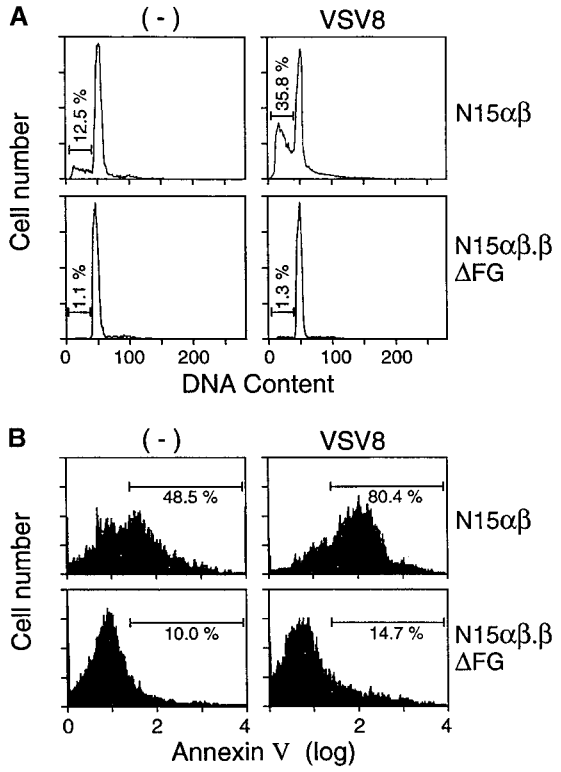

Figure 5. Decreased apoptotic cell death in thymocytes of the N15αβ.βΔFG mice. 7-wk-old N15αβ and N15αβ.βΔFG mice were injected intravenously with 0.5 μg of VSV8 cognate peptide in 0.1 ml PBS. 18 h later, thymocytes were counted and analyzed by flow cytometry for DNA content and annexin V staining to detect apoptotic cells. Treatment of the N15αβ mouse with VSV8 resulted in an dramatic reduction of thymocyte number (without VSV8, 2.07×10^7 cells/mouse; with VSV8, 0.26×10^7 cells/mouse). By contrast, the N15αβ.βΔFG mouse showed no significant changes in the absolute number of thymocytes (without VSV8, 10.4×10^7 cells/mouse; with VSV8, 10.6×10^7 cells/mouse) or their subset distribution after VSV8 injection. (A) Subdiploid DNA-containing thymocytes are decreased in the N15αβ.βΔFG mice. After fixation and permeabilization, total thymocytes from N15αβ and N15αβ.βΔFG mice with or without VSV8 injection were stained with PI and assayed by flow cytometry. The histograms of DNA content on the total thymocytes are shown. The numbers represent the percentages of subdiploid DNA-containing apoptotic thymocytes. (B) Annexin V–positive thymocytes are decreased in the N15αβ.βΔFG mice. Total thymocytes from N15αβ and N15αβ.βΔFG mice with or without VSV8 injection were stained with FITC-conjugated annexin V and assayed by flow cytometry. Dead cells were gated out using PI to reveal the proportion of live thymocytes undergoing early stages of apoptosis. The histograms of annexin V staining on the PI-negative live thymocytes are shown. The numbers represent the percentages of annexin V^+ apoptotic thymocytes.

Collectively, these results suggest that the increase in DP thymocytes in the N15αβ.βΔFG mice can be explained, at least in part, by the reduced sensitivity of those DP thymocytes to undergo peptide-triggered negative selection. Although not shown, higher doses of VSV8 peptide induce apoptotic cell death in both N15αβ and N15αβ.βΔFG thymocytes to a similar extent, suggesting that the N15αβ.βΔFG mice require a larger number of pMHC-ligated TCRs to trigger negative selection. That dexamethasone-induced DNA fragmentation of thymocytes is equivalent in both mouse strains implies no general apoptotic defect in N15αβ.βΔFG animals (data not shown). Note that the observed apoptosis of thymocytes is not secondary to peripheral cytokine production observed in other systems (40) as shown by the rapid kinetics of the N15 TCR tg system and prior parallel FTOC analysis (25, 39).

Impaired Proliferation and Cytokine Production upon Antigen-triggered Stimulation of Naive T Cells in the N15αβ.βΔFG Mice. To examine the role of the Cβ FG loop in mature T cell function, we next tested the antigen responsiveness of N15αβ.βΔFG T cells by culturing lymph node T cells with VSV8 cognate peptide or variant APLs in vitro. To first address whether the Cβ FG loop deletion affects early phases of naive T cell activation, we assessed surface expression of the cell activation "markers," IL-2Rα (CD25) and CD69, which represents a reliable method for determining the number of T cells that are activated in culture (41, 42). The lymph node T cells from N15αβ and N15αβ.βΔFG mice were stimulated in vitro for 18 h with varying molar concentrations of VSV8 or the APL variants, L4 and K1 (26), using irradiated EL-4 cells as $H\text{-}2K^b$-bearing APCs, and then were assayed for the expression of CD25 and CD69 by flow cytometry. As shown in Fig. 6 A, VSV8 peptide was capable of activating virtually almost the same percentages of T cells at the peptide concentration of 10^{-4}–10^{-8} M in both N15αβ and N15αβ.βΔFG mice. However, a very subtle difference is observed in the activation responses of the N15αβ and N15αβ.βΔFG lymph node T cells after stimulation with a lower concentration of VSV8 (10^{-10} M) and more convincingly with the APLs L4 and K1, as assessed by CD69 (Fig. 6 A) and CD25 (data not shown) expression. At peptide concentrations of 10^{-5}–10^{-7} M for L4 and 10^{-4}–10^{-5} M for K1, the percentages of activated T cells from N15αβ mice are slightly higher than those from N15αβ.βΔFG mice; the dose–response curve from N15αβ.βΔFG lymph node cells after treatment with L4 or K1 peptide is shifted to the right by a factor of ~10. These findings indicate that in the mature lymphoid compartment, the early T cell activation by weak agonist ligation is modestly affected by the Cβ FG loop deletion as measured by this assay.

We next examined and compared Ag-induced IFN-γ production and proliferative responses of unprimed naive lymph node T cells from N15αβ and N15αβ.βΔFG mice. As shown in Fig. 6 B, when incubated for 48 h with VSV8 prepulsed EL-4 cells, both the N15αβ and N15αβ.βΔFG lymph node T cells secrete IFN-γ into the culture supernatant at each peptide concentration tested (10^{-5}–10^{-9} M).

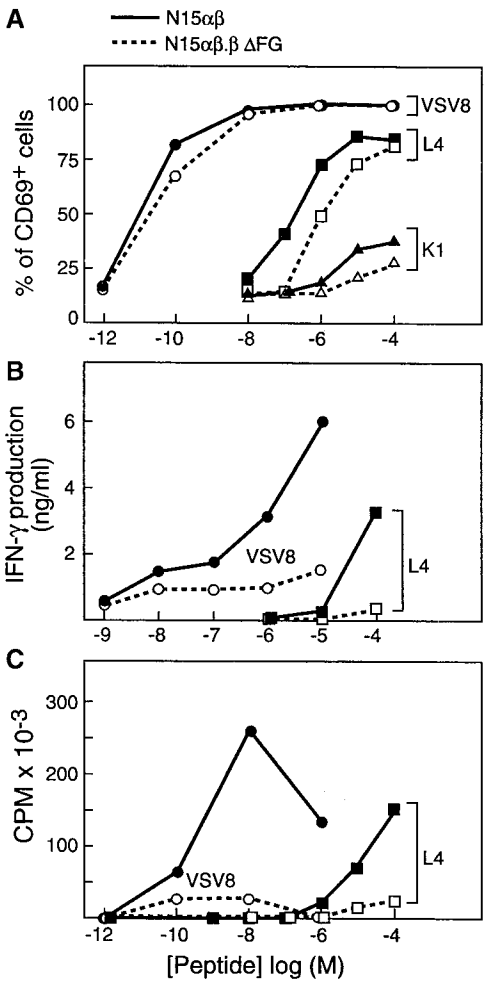

Figure 6. Impaired IFN-γ production and proliferation upon Ag-triggered stimulation of naive T cells in the N15αβ.βΔFG mice. (A) Lymph node T cells (1×10^5 cells) from 8–11-wk-old N15αβ and N15αβ.βΔFG mice were stimulated in vitro with varying molar concentrations of VSV8, L4, or K1 peptide, using irradiated EL-4 cells (2×10^4 cells) as H-2K^b-bearing APCs. After 18 h of culture, cells were stained with Cychrome-anti-CD8, PE-anti-CD25, and biotin-anti-CD69 followed by FITC-streptavidin. Gated CD8$^+$ cells were analyzed and the percentages of CD25- or CD69-positive cells were determined by flow cytometry. The data on CD69 expression only are shown but staining with anti-CD25 mAb showed similar results. (B) Lymph node T cells (1×10^5 cells) from 8–11-wk-old N15αβ and N15αβ.βΔFG mice were incubated with the indicated concentrations of VSV8 and L4 and irradiated K^b-bearing EL-4 cells (2×10^4 cells). 48 h later, supernatants were assayed for IFN-γ production. Mean of duplicate cultures is shown. (C) Lymph node T cells (1×10^5 cells) from 8–11-wk-old N15αβ and N15αβ.βΔFG mice were incubated in vitro with the indicated concentrations of VSV8 and L4, using irradiated EL-4 cells (2×10^4 cells) as H-2K^b-bearing APC. 48 h later, [^{3}H]TdR was pulsed for 18 h and T cell proliferation was judged by [^{3}H]TdR incorporation. Mean of duplicate cultures is shown. Results are representative of four independent experiments.

However, the values of IFN-γ secreted from N15αβ lymph node T cells are higher than those from N15αβ.βΔFG T cells at 10^{-5}–10^{-8} M VSV8. In fact, compared with N15αβ T cells, the dose–response curve from N15αβ.βΔFG lymph node T cells is shifted to the right by a factor of 100–1,000. Furthermore, when incubated with EL-4 cells prepulsed with the weak agonist L4, the N15αβ T cells can produce readily detectable amounts of IFN-γ at a peptide concentration of 10^{-4} M. In contrast, N15αβ.βΔFG lymph node T cells cannot induce IFN-γ production after L4 stimulation at any peptide concentration tested (Fig. 6 B). Similarly, as shown in Fig. 6 C, significant differences are also observed in the IL-2–dependent proliferative responses of the N15αβ and N15αβ.βΔFG lymph node T cells after stimulation with antigenic peptides as assessed by [^{3}H]thymidine incorporation. When N15αβ and N15αβ.βΔFG lymph node T cells are cocultured with irradiated EL-4 cells prepulsed with VSV8 for 48 h, the amounts of incorporated [^{3}H]thymidine in N15αβ.βΔFG lymph node T cells are clearly less than those in N15αβ T cells at peptide concentrations from 10^{-6} to 10^{-10} M (Fig. 6 C). In addition, compared with N15αβ T cells, N15αβ.βΔFG lymph node T cells show significantly decreased proliferative responses to L4 stimulation at peptide concentrations from 10^{-4} to 10^{-6} M, with the dose–response curves from N15αβ.βΔFG lymph node T cells shifted to the right by a factor of 10–100 (Fig. 6 C). Collectively, these results clearly demonstrate that responsiveness to antigenic peptides is impaired in the N15αβ.βΔFG T cells as determined by peptide antigen-specific induction of proliferation and cytokine production.

Discussion

In this study, we generated a TCR β chain mutant (N15βΔFG) in which the entire Cβ FG loop was deleted. The N15βΔFG construct or the normal N15βwt cDNA was then introduced as a transgene into mice and differentiation/functional analysis of thymocytes conducted on the H-2^b background. While N15βΔFG facilitated pre-TCR activity (Fig. 3, and Table I), our analysis reveals a distinct phenotype with respect to effects of the βΔFG mutation on further thymocyte maturation. N15βΔFG tg mice show a statistically significant increase in CD8$^+$ SP thymocytes and lymph node T cells (Table I) in association with alteration of endogenous Vα repertoires (Table II). These results imply that, in balance, enhanced positive selection is favored over negative selection. Given the potential confounding effects of repertoire alteration, we subsequently restricted Vα expression to that of the N15 α subunit on a RAG-2$^{-/-}$ background in a second set of animals. Thus, N15αβ TCR tg RAG-2$^{-/-}$ and N15βΔFG tg RAG-2$^{-/-}$ mice were crossed to generate N15αβ RAG-2$^{-/-}$ and N15αβ.βΔFG RAG-2$^{-/-}$ littermates. N15αβ.βΔFG tg RAG-2$^{-/-}$ mice were striking with regard to an 8–10-fold increase in thymocyte cellularity as a consequence of an increase in DP thymocytes without alteration in cell numbers of DN or CD8$^+$ SP compartments (Fig. 4). This increase was due to reduced negative selection with decreased hypodiploid cellular DNA content constitutively as well as following in vivo VSV8 cognate peptide injection in N15αβ.βΔFG tg RAG-2$^{-/-}$ compared with N15αβ tg RAG-2$^{-/-}$ H-2^b mice (Fig. 5). Annexin V staining further confirmed the re-

duced apoptosis in N15αβ.βΔFG RAG-$2^{-/-}$ versus N15αβ RAG-$2^{-/-}$ mice.

At first glance, these data may appear in conflict with earlier studies by Degermann et al. (43), whose findings indicated that a TCR β chain lacking the identical solvent-exposed Cβ FG loop supported normal αβ T cell development in tg mice as well as normal function in cell transfectants. Their β chain was derived from the 14.3.d TCR specific for $HA_{110–119}$ PR8 influenza hemagglutinin peptide complexed with I-E^d and comprised of Vβ8.2 and Jβ2.1 segments, unlike the N15βΔFG chain derived from the VSV8/K^b-specific N15 $CD8^+$ SP CTL encoded by Vβ5.2 Jβ2.6 segments. In 14.3.d βΔFG tg mice, superantigen-induced proliferation, anti-H-2^d CTL effector function, or helper T cell responses for anti-hapten antibody production were essentially normal. However, given that in the 14.3.d βΔFG tg mice, endogenous TCR α subunits pair with the introduced β transgene product, the biologic system can readily overcome any deficiency mediated by the βΔFG deletion. Hence, polyclonal T cell responses are not a sensitive indicator of the functional consequences of the Cβ FG loop deletion. Consistent with this notion, additional studies by the same authors in 14.3.d βΔFG mice show that αβ T cells coexpressing NK1.1 are severely depleted (44). This is particularly noteworthy, as ~80% of NK1.1 T cells express the invariant (Vα14-Jα281) segment required for their development (45). Thus, even in the RAG-$2^{+/+}$ background, a near single TCR specificity is generated with regard to NK1.1 T cells, permitting the effects of the Cβ FG loop deletion to be recognized. Our results, in conjunction with those of Degermann, imply that the Cβ FG loop is functionally significant for immune recognition-based signaling by both conventional αβ T cells and NK1.1 T cells of pMHC and CD1 specificities, respectively.

Prior mAb epitope mapping analysis showed that one of the two CD3ε subunits within a TCR complex is in close proximity to the TCR Cβ chain FG loop whereas the second CD3ε subunit lies elsewhere. Crystallographic analysis of the N15 TCR αβ heterodimer reveals a striking asymmetry within the constant domain module such that virtually half of the Cβ domain's ABED surface is exposed, yet uninvolved in Cα domain contacts. This asymmetry creates a cavity beneath the β chain with the Cβ ABED surface as a ceiling and the plasma membrane as the floor. The two protruding Cα loops (CD loop and EF loop) plus one Cα (N185) and two Cβ (N121, N186) glycans form one sidewall while the Cβ FG loop and one Cβ (N236) glycan form the second wall of this cave. In structural terms, the role of this extensive FG loop is to further rigidify the interface between Vβ and Cβ domains, thereby limiting the lateral movement of Vβ. In addition, careful analysis of the Cβ FG loop in several TCR structures (22, 28, 30, 46) reveals conservation of the three-dimensional structure of the loop, the adjacent Cβ domain and the cave of both pMHCI- and pMHCII-restricted TCRs in human (29, 30) and mouse (22, 28). Such conservation implies an important role for this structural element on both $CD4^+$ and $CD8^+$ SP T cells. By forming a side wall of the cavity into which a CD3ε subunit of one CD3 heterodimer can insert, the Cβ FG loop presumably stabilizes the interaction between CD3ε and the Tiαβ heterodimer. Not surprisingly, therefore, immunoprecipitation studies using the CD3εγ dimer-specific mAb 7D6 with N15αβ and N15αβΔFG transfectants reveals a markedly weakened association of CD3εγ with the TCR αβ heterodimer and CD3ζ in N15αβΔFG T cells (unpublished data). It is further noteworthy that the loop is negatively charged, perhaps influencing the electrostatics of the TCR surface in a manner similar to an N-linked glycan. Antedating the evolution of the FG loop in higher vertebrates, such a glycan localizes to the same region in primitive species (shark, chicken and axo; data not shown). Although the mouse has an adjacent N-linked glycan as well as the elongated FG loop in its TCR structure, both are not essential since the human TCR lacks an N-linked attachment site.

With these details in mind, we note that the TCR is a largely rigid structure: one component consists of the FG loop–"reinforced" Vβ-Cβ extracellular segment associated via an extensive (~2400 $Å^2$) buried surface interface with the Cα domain of the TCRα subunit, a second component. The Cβ-Cα interface contains multiple rigidifying salt bridges. Hence, the Vβ-Cβ-Cα domains form a single conformationally rigid module. This Vβ-Cβ-Cα module in turn is noncovalently associated with the CD3εγ and/or CD3εδ heterodimers such that the glycosylated CD3γ and CD3δ subunits extend away from the TCR heterodimer while the two nonglycosylated CD3ε subunits are proximal. NMR structural studies show that CD3ε and CD3γ (and by extension CD3εδ) adopt C2-set IgSF folds, forming a stable heterodimeric complex by parallel strand pairing (G strand) and hydrophobic interaction (24). The CD3ε-CD3γ G strand pairing presumably creates a rodlike connector, permitting displacement of transmembrane helices of CD3εγ and CD3εδ upon TCR triggering, leading to intracellular kinase-dependent events and resulting in T lineage activation. Removal of the Cβ FG loop, by eliminating one wall of the cave in the Cβ domain would reduce one key component of the rigidifying architecture such that signaling might be impaired. Hence the altered negative selection in DP thymocytes of the N15αβ.βΔFG animals and the reduced capacity of their $CD8^+$ SP lymph node T cells to proliferate to cognate antigens and APL are anticipated sequelae. That polyclonal thymocytes and αβ T cells in βΔFG tg mice (i.e. RAG-$2^{+/+}$) can overcome this block, implies either that compensatory adaptations in the TCRα subunit or elsewhere readily occur or that additional protein interactions among TCR subunits (for example, within their transmembrane segments) maintain TCR-based signaling even in the absence of FG loop constraint. These possibilities are not mutually exclusive.

The prominent effect of the βΔFG transgene in N15αβ.βΔFG RAG-$2^{-/-}$ mice is the marked inefficiency of negative selection processes compared with that of N15αβ RAG-$2^{-/-}$ mice. Interestingly, the Cβ FG loop deletion impairs negative selection without diminishing the capacity of DP thymocytes to differentiate to CD8 SP thy-

mocytes; hence, the number of $CD8^+$ SP thymocytes in N15αβ.βΔFG RAG-$2^{-/-}$ H-2^b and N15αβ RAG-$2^{-/-}$ H-2^b littermates is identical. In general, pMHC ligands of stronger affinity are negatively selecting while those with weaker affinity for a given TCR are positively selecting (for reviews, see references 47 and 48). Given that the Cβ FG loop deletion will reduce rigidification and likely attenuate signaling from negatively selecting ligands, this result is not surprising. In contrast, positive selection must not be attenuated below a threshold required for initiating effective survival signaling. As other studies have demonstrated that positive and negative selection are under the control of different signaling pathways (for reviews, see references 38 and 49), this differential concept is entirely tenable. Nevertheless, in N15αβ.βΔFG RAG-$2^{-/-}$ mice, the numbers of $CD8^+$ SP lymph node T cells are somewhat reduced compared with N15αβ RAG-$2^{-/-}$ mice on the same H-2 background. This observation in conjunction with increased HSA and PNA staining of $CD8^+$ SP thymocytes in N15αβ.βΔFG RAG-$2^{-/-}$ mice (data not shown) suggests that positive selection may not be entirely unaffected by the CβΔ FG mutation.

The pre-TCR consists of a TCRβ chain disulfide-bonded to the thymus-restricted pTα subunit expressed on DN thymocytes in association with CD3ε heterodimers and CD3ζ homodimers (34, 50). Although the single Ig-like ectodomain of pTα bears only 12% homology to TCR Cα, key residues participating in the formation of the rigid interface between Cα and Cβ are preserved (22). This structural conservation suggests that the heterodimeric interface of pTα-Cβ is similar to the interface of Cα-Cβ. From this conserved feature, we have inferred that a CD3ε heterodimer slots into a pre-TCR cave comparable to that created within the TCR. That a CD3ε knockout mutation disrupts pTα function (51) is consistent with this view. Furthermore, given that a CD3γ knockout also disrupts pre-TCR function (52), it is tempting to speculate that CD3εγ is the cave-associated CD3ε heterodimer. Limited glycosylation of CD3γ relative to CD3δ allows for ready modeled docking of the CD3εγ but not CD3εδ heterodimer at this cavity while still accommodating H57 mAb binding (unpublished results). Three additional facts also support the presumptive CD3εγ localization. First, it is known from chain association studies that CD3εδ pairs with TCRα whereas the CD3εγ heterodimer binds to TCRβ (53). Second, these experiments show that CD3ε and TCRβ interact via their respective ectodomains whereas the associations of the CD3γ, δ, and ζ components with TCR α and β are mediated via their transmembrane regions. Third, chemical cross-linking experiments in man and mouse imply proximity of TCRβ and CD3γ (18, 54). The above results notwithstanding, verification of these predictions still requires definitive structural elucidation.

The inability of the Cβ FG loop deletion to influence the function of the pre-TCR is consistent with recent transgenic experiments in the pTα$^{-/-}$ background: pTα constructs lacking both the ectodomain and much of the cytoplasmic tail still support pre-TCR function (55). These data imply that pTα stabilizes the pre-TCR predominantly via transmembrane interactions, with CD3ε heterodimer association not singularly dependent on the cave for pre-TCR function. Further support for this notion comes from three other observations: (a) mice transgenic for a TCRβ chain lacking the Vβ domain support DN to DP transition (56); (b) pTα and TCRβ chains lacking their respective Ig-like domains still facilitate thymic differentiation in RAG-deficient mice (57); and (c) mutational analysis of the two tyrosines in the TCRβ transmembrane region show that even conservative tyrosine to phenylalanine changes disrupt thymocyte survival, proliferation, and differentiation (58), further underscoring the importance of the transmembrane segment for pre-TCR function. Alterations within the TCR ectodomains are less well tolerated with regard to αβTCR function, significantly impinging on TCR activity. For example, Cβ FG loop deletion reduces the efficiency of negative selection in N15αβ.βΔFG RAG-$2^{-/-}$ mice. Mutations of the TCRα chain connecting peptide profoundly affect positive selection. The latter occurs through attenuation of ERK activation and a reduction of activated lck, Zap-70, phospho-CD3ζ, and phospho-LAT within lipid rafts (59). A similar phenotype with equivalent biochemical signaling aberrations is observed in CD3δ$^{-/-}$ mice (60). If CD3εγ maps to the TCRβ side and CD3εδ to the TCRα side of the αβ TCR complex, these findings can be rationalized.

In N15αβ.βΔFG RAG-$2^{-/-}$ H-2^b mice, the level of N15 TCR as judged by both MR9.4 (anti-Vβ5) or R53 (anti-Vβ clonotype) is virtually identical to that found on T cells of N15αβ RAG-$2^{-/-}$ H-2^b mice. However, in the former case, ~50% of TCRs are wild-type and 50% incorporate the mutant βΔFG subunit. Yet mature $CD8^+$ SP T cell function is significantly reduced in N15αβ.βΔFG RAG-$2^{-/-}$ mice. Thus, despite half of the TCRs being wild-type in structure, functional activation of these T cells vis-a-vis cytokine production or proliferation is dramatically reduced. In contrast, tetracycline regulatable TCR transgene expression shows that cells expressing as few as 1/20 of the normal levels of TCRs preserve their functional activity (61). Thus, paradoxically, the presence of TCRs with the βΔFG subunit is more detrimental to TCR-triggered activation than the complete absence of wild-type TCRs. Although the basis for this disparity remains to be elucidated, N15αβ.βΔFG TCRs may dysregulate wt TCRs by activating inhibitory pathways (phosphatases or others) in the absence of productive stimulation.

These data indicate an important functional role for the Cβ FG loop in both thymic negative selection and mature T cell activation, T lineage activities requiring threshold stimulation to achieve a stringent set point. On the other hand, positive selection is only modestly altered. In view of evidence that positive selection requirements vis-a-vis pMHC interaction are less arduous with regard to affinity and avidity than those for negative selection (47, 48), this result is perhaps not surprising. Thus, attendant reduction in signaling strength through TCRs incorporating mutant βΔFG subunits may still be sufficient to achieve the more

"relaxed" set point threshold for successful positive selection. Apparently, structural features of the αβ TCR have evolved to facilitate the "multi-tasking" requirements of TCR signaling function during development and mature T cell function. In sum, TCRβ-linked transduction events are more critically involved in negative selection while it appears that TCRα-linked transduction processes are key for positive selection.

This work was supported by National Institutes of Health grants AI19807 to E.L. Reinherz, GM56008 to J.-H. Wang, and AI39098 to H.-C. Chang.

Submitted: 23 January 2002
Revised: 29 March 2002
Accepted: 15 April 2002

References

1. Meuer, S.C., D.A. Cooper, J.C. Hodgdon, R.E. Hussey, K.A. Fitzgerald, S.F. Schlossman, and E.L. Reinherz. 1983. Identification of the antigen/MHC receptor on human inducer T lymphocytes. *Science*. 222:1239–1242.
2. Marrack, P., and J. Kappler. 1986. The antigen-specific, major histocompatibility complex-restricted receptor on T cells. *Adv. Immunol*. 38:1–30.
3. Clevers, H., B. Alarcon, T. Wileman, and C. Terhorst. 1988. The T cell receptor/CD3 complex: A dynamic protein ensemble. *Annu. Rev. Immunol*. 6:629–662.
4. Davis, M.M., and P.J. Bjorkman. 1988. T cell antigen receptor genes and T cell recognition. *Nature*. 334:395–402.
5. Ashwell, J.D., and R.D. Klausner. 1990. Genetic and mutational analysis of the T cell antigen receptor. *Annu. Rev. Immunol*. 8:139–167.
6. Kaufman, S.H.E. 1996. γ/δ and other unconventional T lymphocytes: What do they see and what do they do? *Proc. Natl. Acad. Sci. USA*. 93:2272–2279.
7. Reth, M. 1989. Antigen receptor tail clue. *Nature*. 338:383–384.
8. Weiss, A., and D.R. Littman. 1994. Signal transduction by lymphocyte antigen receptors. *Cell*. 76:263–274.
9. Cambier, J.C. 1995. Antigen and Fc receptor signaling. The awesome power of the immunoreceptor tyrosine-based activation motif (ITAM). *J. Immunol*. 155:3281–3285.
10. Letourneur, F., and R.D. Klausner. 1992. Activation of T cells by a tyrosine kinase activation domain in the cytoplasmic tail of CD3ε. *Science*. 255:79–82.
11. Ravichandran, K.S., K.K. Lee, Z. Songyang, L.C. Cantley, P. Burn, and S.J. Burakoff. 1993. Interaction of Shc with the ζ chain of the T cell receptor upon T cell activation. *Science*. 262:902–905.
12. Exley, M., L. Varticovski, M. Peter, J. Sancho, and C. Terhorst. 1994. Association of phosphatidylinositol 3-kinase with a specific sequence of the T cell receptor ζ chain is dependent on T cell activation. *J. Biol. Chem*. 269:15140–15146.
13. Isakov, N., R.L. Wange, W.H. Burgess, J.D. Watts, R. Aebersold, and L.E. Samelson. 1995. ZAP-70 binding specificity to T cell receptor tyrosine-based activation motifs: the tandem SH2 domains of ZAP-70 bind distinct tyrosine-based activation motifs with varying affinity. *J. Exp. Med*. 181:375–380.
14. Osman, N., H. Turner, S. Lucas, K. Reif, and D.A. Cantrell. 1996. The protein interactions of the immunoglobulin receptor family tyrosine-based activation motifs present in the T cell receptor ζ subunits and the CD3 γ, δ and ε chains. *Eur. J. Immunol*. 26:1063–1068.
15. Sunder-Plassmann, R., F. Lialios, M. Madsen, S. Koyasu, and E.L. Reinherz. 1997. Functional analysis of immunoreceptor tyrosine-based activation motif (ITAM)-mediated signal transduction: the two YxxL segments within a single CD3ζ-ITAM are functionally distinct. *Eur. J. Immunol*. 27:2001–2009.
16. Alarcon, B., B. Berkhout, J. Breitmeyer, and C. Terhorst. 1988. Assembly of the human T cell receptor-CD3 complex takes place in the endoplasmic reticulum and involves intermediary complexes between the CD3-γδε core and single T cell receptor α or β chains. *J. Biol. Chem*. 263:2953–2961.
17. Baniyash, M., P. Garcia-Morales, J.S. Bonifacino, L.E. Samelson, and R.D. Klausner. 1988. Disulfide linkage in the ζ and η chains of the T cell receptor. *J. Biol. Chem*. 263: 9874–9878.
18. Koning, F., W.L. Maloy, and J.E. Coligan. 1990. The implications of subunit interactions for the structure of the T cell receptor-CD3 complex. *Eur. J. Immunol*. 20:299–305.
19. de la Hera, A., U. Muller, C. Olsson, S. Isaaz, and A. Tunnacliffe. 1991. Structure of the T cell antigen receptor (TCR): Two CD3ε subunits in a functional TCR/CD3 complex. *J. Exp. Med*. 173:7–17.
20. Manolios, N., F. Letourneur, J.S. Bonifacino, and R.D. Klausner. 1991. Pairwise, cooperative and inhibitory interactions describe the assembly and probable structure of the T cell antigen receptor. *EMBO J*. 10:1643–1651.
21. Punt, J.A., J.L. Roberts, K.P. Kearse, and A. Singer. 1994. Stoichiometry of the T cell antigen receptor (TCR) complex: each TCR/CD3 complex contains one TCR α, one TCR β, and two CD3ε chains. *J. Exp. Med*. 180:587–593.
22. Wang, J., K. Lim, A. Smolyar, M.-K. Teng, J.-H. Liu, A.G.T. Tse, J. Liu, R.E. Hussey, Y. Chishti, C.T. Thomson, et al. 1998. Atomic structure of an αβ T cell receptor (TCR) heterodimer in complex with an anti-TCR Fab fragment derived from a mitogenic antibody. *EMBO J*. 17:10–26.
23. Ghendler, Y., A. Smolyar, H.-C. Chang, and E.L. Reinherz. 1998. One of the CD3ε subunits within a T cell receptor complex lies in close proximity to the Cβ FG loop. *J. Exp. Med*. 187:1529–1536.
24. Sun, Z.-Y.J., K.S. Kim, G. Wagner, and E.L. Reinherz. 2001. Mechanisms contributing to T cell receptor signaling and assembly revealed by the solution structure of an ectodomain fragment of the CD3εγ heterodimer. *Cell*. 105: 913–923.
25. Ghendler, Y., R.E. Hussey, T. Witte, E. Mizoguchi, L.K. Clayton, A.K. Bhan, S. Koyasu, H.C. Chang, and E.L. Reinherz. 1997. Double positive T cell receptor^{high} thymocytes are resistant to peptide/major histocompatibility complex ligand-induced negative selection. *Eur. J. Immunol*. 27:2279–2289.
26. Ghendler, Y., M.-K. Teng, J.-H. Liu, T. Witte, J. Liu, K.S. Kim, P. Kern, H.-C. Chang, J.-H. Wang, and E.L. Reinherz. 1998. Differential thymic selection outcomes stimulated by focal structural alteration in peptide/major histocompatibility complex ligands. *Proc. Natl. Acad. Sci. USA*. 95:10061–10066.
27. Kabat, E.A., T.T. Wu, H.M. Perry, K.S. Gottesman, and C. Faeller. 1991. Sequences of proteins of immunological inter-

est. *US Dept. of Health and Human Services*.
28. Garcia, K.C., M. Degano, R.L. Stanfield, A. Brunmark, M.R. Jackson, P.A. Peterson, L. Teyton, and I.A. Wilson. 1996. An αβ T cell receptor structure at 2.5Å and its orientation in the TCR-MHC complex. *Science*. 274:209–219.
29. Ding, Y.H., K.J. Smith, D.N. Garboczi, U. Utz, W.E. Biddison, and D.C. Wiley. 1998. Two human T cell receptors bind in a similar diagonal mode to the HLA-A2/Tax peptide complex using different TCR amino acids. *Immunity*. 8:403–411.
30. Hennecke, J., A. Carfi, and D.C. Wiley. 2000. Structure of a covalently stabilized complex of a human αβ T cell receptor, influenza HA peptide and MHC class II molecule, HLA-DR1. *EMBO J.* 19:5611–5624.
31. Chang, H.-C., A. Smolyar, R. Spoerl, T. Witte, Y. Yao, E.C. Goyarts, S.G. Nathenson, and E.L. Reinherz. 1997. Topology of T cell receptor-peptide/class I MHC interaction defined by charge reversal complementation and functional analysis. *J. Mol. Biol.* 271:278–293.
32. Kubo, R.T., W. Born, J.W. Kappler, P. Marrack, and M. Pigeon. 1989. Characterization of a monoclonal antibody which detects all murine αβ T cell receptors. *J. Immunol.* 142:2736–2742.
33. Balomenos, D., R.S. Balderas, K.P. Mulvany, J. Kaye, D.H. Kono, and A.N. Theofilopoulos. 1995. Incomplete T cell receptor Vβ allelic exclusion and dual Vβ expressing cells. *J. Immunol.* 155:3308–3312.
34. Saint-Ruf, C., K. Ungewiss, M. Groettrup, L. Bruno, H.J. Fehling, and H. von Boehmer. 1994. Analysis and expression of a cloned pre-T cell receptor gene. *Science*. 266:1208–1212.
35. Goldrath, A.W., and M.J. Bevan. 1999. Selecting and maintaining a diverse T cell repertoire. *Nature*. 402:255–262.
36. Shinkai, Y., S. Koyasu, K.-I. Nakayama, K.M. Murphy, D.Y. Loh, E.L. Reinherz, and F.W. Alt. 1993. Restoration of T cell development in RAG-2 deficient mice by functionally rearranged TCR transgenes. *Science*. 259:822–825.
37. Freitas, A.A., and B. Rocha. 2000. Population biology of lymphocytes: the fight for survival. *Annu. Rev. Immunol.* 18: 83–111.
38. Sebzda, E., S. Mariathasan, T. Ohteki, R. Jones, M.F. Bachmann, and P.S. Ohashi. 1999. Selection of the T cell repertoire. *Annu. Rev. Immunol.* 17:829–874.
39. Clayton, L.K., Y. Ghendler, E. Mizoguchi, R.J. Patch, T.D. Ocain, K. Orth, A.K. Bhan, V.M. Dixit, and E.L. Reinherz. 1997. T cell receptor ligation by peptide/MHC induces activation of a caspase in immature thymocytes: the molecular basis of negative selection. *EMBO J.* 16:2282–2293.
40. Martin, S., and M.J. Bevan. 1997. Antigen-specific and non-specific deletion of immature cortical thymocytes caused by antigen injection. *Eur. J. Immunol.* 27:2726–2736.
41. Waldmann, T.A. 1989. The multi-subunit interleukin-2 receptor. *Annu. Rev. Biochem.* 58:875–911.
42. Testi, R., D. D'Ambrosio, R. DeMaria, and A. Santoni. 1994. The CD69 receptor: a multipurpose cell surface trigger for hematopoietic cells. *Immunol. Today*. 15:479–483.
43. Degermann, S., G. Sollami, and K. Karjalainen. 1999. T cell receptor β chain lacking the large solvent-exposed Cβ FG loop supports normal α/β T cell development and function in transgenic mice. *J. Exp. Med.* 189:1679–1684.
44. Degermann, S., G. Sollami, and K. Karjalainen. 1999. Impaired NK1.1 T cell development in mice transgenic for a T cell receptor β chain lacking the large, solvent-exposed Cβ FG loop. *J. Exp. Med.* 190:1357–1362.
45. Lantz, O., and A. Bendelac. 1994. An invariant T cell receptor α chain is used by a unique subset of major histocompatibility complex class I specific $CD4^+$ and $CD4^-8^-$ T cells in mice and humans. *J. Exp. Med.* 180:1097–1106.
46. Garcia, K.C., M. Degano, L.R. Pease, M. Huang, P.A. Peterson, L. Teyton, and I.A. Wilson. 1998. Structural basis of plasticity in T cell receptor recognition of a self peptide-MHC antigen. *Science*. 279:1166–1172.
47. Ashton-Rickardt, P.G., and S. Tonegawa. 1994. A differential avidity model for T cell selection. *Immunol. Today*. 15: 362–366.
48. Alam, S.M., P.J. Travers, J.L. Wung, W. Nasholds, S. Redpath, S.C. Jameson, and N.R.J. Gascoigne. 1996. T-cell-receptor affinity and thymocyte positive selection. *Nature*. 381:616–620.
49. Hogquist, K.A. 2001. Signal strength in thymic selection and lineage commitment. *Curr. Opin. Immunol.* 13:225–231.
50. von Boehmer, H., I. Aifantis, O. Azogui, J. Feinberg, C. Saint-Ruf, C. Zober, C. Garcia, and J. Buer. 1998. Crucial function of the pre-T cell receptor (TCR) in TCR β selection, TCR β allelic exclusion and αβ versus γδ lineage commitment. *Immunol. Rev.* 164:111–119.
51. Malissen, M., A. Gillet, L. Ardouin, G. Bouvier, J. Trucy, P. Ferrier, E. Vivier, and B. Malissen. 1995. Altered T cell development in mice with a targeted mutation of the CD3ε gene. *EMBO J.* 14:4641–4653.
52. Haks, M.C., P. Krimpenfort, J. Borst, and A.M. Kruisbeek. 1998. The CD3γ chain is essential for development of both the TCRαβ and TCRγδ lineages. *EMBO J.* 17:1871–1882.
53. Manolios, N., O. Kemp, and Z.G. Li. 1994. The T cell antigen receptor α and β chains interact via distinct regions with CD3 chains. *Eur. J. Immunol.* 24:84–92.
54. Brenner, M.B., I.S. Trowbridge, and J.L. Strominger. 1985. Crosslinking of human T cell receptor proteins: association between the T cell idiotype β subunit and the T3 glycoprotein heavy subunit. *Cell*. 40:183–190.
55. Gibbons, D., N.C. Douglas, D.F. Barber, Q. Liu, R. Sullo, L. Geng, H.J. Fehling, H. von Boehmer, and A.C. Hayday. 2001. The biological activity of natural and mutant pTα alleles. *J. Exp. Med.* 194:695–703.
56. Ossendorp, F., H. Jacobs, G. van der Horst, E. de Vries, A. Berns, and J. Borst. 1992. T cell receptor lacking the αβ chain V domain can be expressed at the cell surface but prohibits T cell maturation. *J. Immunol.* 148:3714–3722.
57. Irving, B.A., F.W. Alt, and N. Killeen. 1998. Thymocyte development in the absence of pre-T cell receptor extracellular immunoglobulin domains. *Science*. 280:905–908.
58. Spain, L.M., and P. Liu. 2002. TCRβ transmembrane tyrosines are required for pre-TCR function. *J. Immunol.* 168: 127–133.
59. Werlen, G., B. Hausmann, and E. Palmer. 2000. A motif in the αβ T cell receptor controls positive selection by modulating ERK activity. *Nature*. 406:422–426.
60. Delgado, P., E. Fernandez, V. Dave, D. Kappes, and B. Alarcon. 2000. CD3δ couples T cell receptor signaling to ERK activation and thymocyte positive selection. *Nature*. 406:426–430.
61. Labrecque, N., L.S. Whitfield, R. Obst, C. Waltzinger, C. Benoist, and D. Mathis. 2001. How much TCR does a T cell need? *Immunity*. 15:71–82.
62. Evans, S.V. 1993. SETOR: hardware lighted three dimensional solid model representation of macromolecules. *J. Mol. Graph.* 11:134–138.